Comparison of Bidirectional Reflectance Distribution Function Scales Over the Hemisphere

ELLIE MOLLOY,[1,*] HEATHER PATRICK,[2] KAI-OLAF HAUER[3], DIRK HÜNERHOFF[3], AND TATJANA QUAST[3]

[1] *Measurement Standards Laboratory of New Zealand, Lower Hutt, New Zealand*
[2] *National Institute of Standards and Technology, Gaithersburg, United States of America*
[3] *Physikalisch-Technische Bundesanstalt, Braunschweig, Germany*
[*] *ellie.molloy@measurement.govt.nz*

Abstract:
Measurements of both hemispherical and directional diffuse reflectance are regularly used in a range of industries to aid in quantifying the appearance of different objects, with increasing demand for metrologically traceable measurements of these quantities. While there have been several comparisons of diffuse reflectance scales, there have been fewer comparisons of bidirectional reflectance distribution function (BRDF) scales between national metrology institutes, and BRDF comparisons have been restricted to a narrow range of measurement geometries. This paper expands upon previous work by comparing BRDF scales over the whole detection hemisphere with normal incidence and comparing diffuse reflectance values calculated by integrating these BRDF measurements with integrating sphere-based diffuse reflectance measurements. The results of this comparison demonstrate the current limits of agreement between BRDF measurements and highlight the discrepancy between goniospectrophotometric and integrating sphere-based realisations of diffuse reflectance.

1. Introduction

Accurate measurements of hemispherical reflectance and the bidirectional reflectance distribution function (BRDF) are important for a range of different industries, including remote sensing, computer graphics, and lighting design. Quantifying the scattering of light off different materials allows us to describe the colour, texture, gloss, and transparency of objects around us. The need for metrologically traceable measurements of 'appearance' has been growing as it is known that visual effects have an influence on a customer's judgement of the quality and acceptability of manufactured products.

Measurements of BRDF are carried out by national metrology institutes (NMIs) using instruments called goniospectrophotometers, which can vary the angles of incidence and reflectance of light on a sample over a range of wavelengths. At some NMIs, the scale of hemispherical diffuse reflectance is realised using a goniospectrophotometer by integrating measurements of BRDF made over the hemisphere. Other NMIs realise the scale of hemispherical diffuse reflectance using an integrating sphere. While there have been several key comparisons arranged by the Consultative Committee of Photometry and Radiometry (CCPR) comparing measurements of hemispherical diffuse reflectance, there has been no key comparison for BRDF.

Outside of the framework of the CCPR, there have been a few bilateral and multilateral comparisons of BRDF carried out between NMIs. In 2015, the National Institute of Standards and Technology (NIST) and the *Physikalisch-Technische Bundesanstalt* (PTB) compared their scales for one specific geometry [1]. There have also been two multilateral comparisons carried out between NMIs within European Metrology Research Programme projects [2, 3], which both focused on only a few geometries. Both of these comparisons demonstrated a systematic difference between the BRDF scales realised at the Measurement Standards Laboratory of New Zealand (MSL) and PTB.

This paper describes a comparison between the BRDF scales of MSL, NIST, and PTB with normal incidence over the whole detection hemisphere for both a white and grey sample. By measuring the BRDF over the hemisphere, the hemispherical diffuse reflectance can be calculated and compared to measurements made using integrating spheres. All three NMIs made BRDF measurements, and both PTB and NIST also measured the hemispherical diffuse reflectance using integrating spheres. Including NIST, PTB, and MSL in the comparison and measuring over a full detection hemisphere enabled us to broaden the investigation of previously observed scale differences between PTB and MSL, and to compare measurements with the BRDF scale of NIST, who did not participate in the European Metrology Research Programme projects.

Section 2 of this paper describes the measurand and introduces the experimental setup at each laboratory. Then in Section 3, a summary of the BRDF measurements is presented, along with a description of the measurement uncertainties. Section 4 describes the hemispherical diffuse reflectance measurements and compares the integrated BRDF values with measurements made using integrating spheres. Finally, some conclusions reached during this work are discussed in Section 5.

2. Measurements

This work was carried out using two sintered polytetrafluoroethylene (PTFE) samples, with nominal reflectances of 99% and 40%, referred to as white and grey, respectively. This type of material is diffuse, with only a small specular component. It is also isotropic, with little change in the BRDF as a function of the azimuthal angle. The measurement geometry is defined in Figure 1. Each laboratory made measurements of BRDF with 0° incidence over the whole detection hemisphere (θ_d from 10° to 80° in 10° steps with an additional measurement at 45° and ϕ_d from 0° to 315° in 45° steps). The 90° azimuthal direction ($\phi_d = 90°$) is along the positive y direction shown in the figure. Measurements were reported for a 10 mm (NIST) or 20 mm

(MSL and PTB) diameter area in the centre of the sample using 550 nm unpolarised light. Prior to this comparison, measurements by MSL and PTB showed minimal sensitivity of the samples to measurement area in this range of beam diameters.

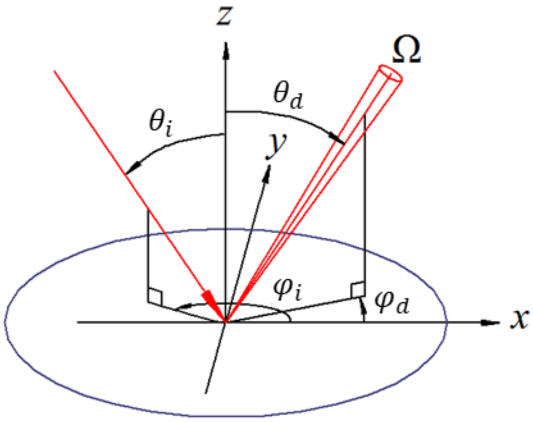

Figure 1. Definition of the measurement geometry. The positive *z* direction is normal to the face of the sample. The subscript i denotes the incident direction and subscript d the reflected direction.

The BRDF, f_r, is defined as the ratio of the reflected radiance L_r from the surface of the sample to the irradiance E_i incident on the sample [4],

$$f_r(\theta_i, \phi_i, \theta_d, \phi_d, \lambda) = \frac{L_r(\theta_i,\phi_i,\theta_d,\phi_d,\lambda)}{E_i(\theta_i,\varphi_i,\lambda)}, \quad (1)$$

where λ is the wavelength.

The BRDF can be measured absolutely using either the under-illumination or over-illumination method. When using the under-illumination method, the sample is illuminated using a relatively small spot on the sample and the amount of light scattered into a known solid angle is measured [4]:

$$f_r = \frac{\Phi_d}{\Phi_i} \frac{1}{\Omega_d \cos\theta_d}, \quad (2)$$

where Φ_d is the reflected radiant flux, Φ_i is the incident radiant flux, and Ω_d is the solid angle of detection. In the over-illumination method, the sample is illuminated using uniform irradiance over the entire sample and the radiance of the sample is measured:

$$f_r = \frac{L_d}{L_i} \frac{1}{\Omega_i \cos\theta_i}, \quad (3)$$

where L_i is the radiance of the source and Ω_i is the solid angle of illumination. PTB measures BRDF using the over-illumination method, while both MSL and NIST use the under-illumination method.

Integrating sphere measurements were made at NIST and PTB. At NIST, measurements were made in the 8°/di geometry, while at PTB measurements were made in the d/0° geometry. For white PTFE samples, it has previously been demonstrated that the diffuse reflectance measured in these geometries are equivalent [5].

2.1 Measurement Setups

The measurement setups at each laboratory are described in the following subsections. Table 1 summarises the measurement parameters for the goniospectrophotometers at each laboratory and Table 2 summarises the measurement parameters for the integrating spheres used by NIST and PTB.

Table 1. Measurement parameters for the goniospectrophotometers used in this comparison.

Parameter	MSL	NIST	PTB
Spectral determination	Monochromatic source, broadband detection	Monochromatic source, broadband detection	Broadband source, monochromatic detection
Source	Supercontinuum	Xenon laser driven light source	Halogen-sphere radiator
Detector	Si photodiode	UV-enhanced Si photodiode	Si photodiode
Bandwidth	2 nm	14 nm	2 nm
Aperture distance	496 mm	657.6 mm	783.8 mm
Aperture area	735.4 mm^2	1128.6 mm^2	1257.34 mm^2
Beam diameter	20 mm	10 mm	20 mm
Illumination scheme	Under-illumination	Under-illumination	Over-illumination

Table 2. Measurement parameters for the integrating spheres used in this comparison.

Parameter	NIST	PTB
Sphere geometry	8°/di	d/0°
Scale realisation	Van den Akker	Korte–Schmidt
Sphere inner diameter	290 mm	500 mm
Coating Material	PTFE	$BaSO_4$
Sphere port diameter	37 mm	Not applicable
Beam diameter	10 mm	20 mm
Spectral determination	Monochromatic source, broadband detection	Broadband source, monochromatic detection
Source	Xenon laser driven light source	100 W quartz halogen lamp
Detector	UV-enhanced Si photodiode	Si photodiode
Bandwidth	14 nm	3 nm

2.1.1 MSL

The goniospectrophotometer at MSL consists of a three-axis rotation stage positioned in the centre of a slew ring, carrying the detector [6]. MSL uses the under-illumination method, with collimated and polarised light from a supercontinuum source coupled to a monochromator with a 2 nm bandwidth beam illuminating the sample. A variable aperture in the beam path allows the beam size on the sample to be varied. The measurements presented here were performed with a 20 mm diameter beam on the sample. The stability of the source is monitored during measurements, and the radiant flux reflected off the sample is detected using a silicon photodiode detector without any further wavelength or polarisation filtering. The solid angle of detection can be varied by adjusting an aperture on the front of the detector. These measurements were carried out using an aperture with a nominal diameter of 30.6 mm at a nominal distance of 496 mm from the sample. Measurements are made using vertically and horizontally polarised light, which are averaged to obtain the BRDF for unpolarised incident light.

2.1.2 NIST

BRDF measurements at NIST were made using the NIST Robotic Optical Scattering Instrument (ROSI) and integrating sphere measurements were made using the Reference Integrating Sphere (RIS). ROSI and the RIS are described in [7] and measurement parameters are given in Tables 1 and 2. For both systems, the illumination was produced by focusing light from a xenon laser-driven light source into a monochromator. The 550 nm output was chopped, polarised and projected to either ROSI or the RIS.

The ROSI goniospectrophotometer consists of a robotic-arm-based goniometer that holds the sample at the centre of rotation of a receiver arm attached to a rotation stage. BRDF measurements in ROSI are made using the under-illumination method with a 10 mm diameter beam on the sample. The robot goniometer was aligned with the front surface of the sample normal to the incident beam and centred on the axis of rotation of the receiver arm. The receiver consists of an aperture, focusing lens, and ultraviolet-enhanced silicon photodiode. Measurements are absolute: the receiver can be positioned to measure the incident radiant flux or the reflected radiant flux. Signals are collected using lock-in detection, and the stability of the source is monitored during measurements to correct for any drift in the incident beam. The samples were measured at the angles listed in Section 2 for polarisations of the illumination beam both parallel and perpendicular to the plane of incidence and the values for both polarisations were averaged to yield f_r for unpolarised incident light.

The integrating sphere (RIS) measures directional-hemispherical reflectance in the 8°/di geometry, where 8° is the incident polar angle on the sample and di refers to hemispherical collection with the specular component included. The sphere geometry is given in Table 2. The samples were measured using linear polarisations of the illumination beam both parallel and perpendicular to the plane of incidence and the values measured for both polarisations were averaged to yield diffuse reflectance for unpolarised incident light. The RIS uses a substitution method, requiring comparison to a standard with a calibrated 8°/di spectral reflectance factor. The standard was pressed polytetrafluoroethylene (PTFE), and its 8°/di reflectance factor was determined using the absolute method of Van den Akker [7].

2.1.3 PTB

The reference gonioreflectometer at PTB, constructed in its original version by A Höpe [8] and modified since then in some detail, is a measurement facility dedicated to the determination of the BRDF. The sample under test is placed on a five-axis robot arm in the centre of the apparatus. For sample illumination, a special integrating sphere radiation source is mounted on a large rotation stage and can be rotated around the sample. The reflected radiation is collected through a fixed detection path consisting of the imaging optics, a double-monochromator, and a detection system (electronics plus detector). On the detection side, four different detector types can be used: a solar blind channel photomultiplier, a yellow enhanced channel photomultiplier, a silicon photodiode (which was used for the measurements presented in this publication), and a cooled InGaAs photodiode. All the signals are detected with a pico-ammeter. This combination of robotic sample holder, mobile light source, and fixed detection allows highly precise measurements of the BRDF in almost any arbitrary bidirectional geometry, in-plane as well as out-of-plane, related to the plane spanned by the direction of illumination and the normal on the sample.

PTB's gonioreflectometer employs the over-illumination method. A homogeneous radiation with high output and a highly Lambertian beam profile is required. Radiation is generated by a sphere radiator equipped with a 400 W quartz-tungsten halogen lamp [9]. This reliable halogen-sphere radiator (Halogen-SR) generates a spatially homogeneous, unpolarised irradiation and a high output in the visible and near-infrared spectral range. The reflected radiation from a circular area of 20 mm diameter in the centre of the sample is collected and spectral selection with a 2 nm bandwidth takes place in the detection path.

For measurements in hemispherical–directional geometries, i.e., diffuse irradiation from the half-sphere onto the sample with subsequent measurement of the directed reflection, an integrating sphere is used. The measurement procedure used for this purpose is the Korte–Schmidt method, which was developed at PTB [10]. The reflection characteristic measured in this case is the hemispherical reflectance in the geometry d/0°.

In the case of the Korte–Schmidt method, the sample to be measured is mounted at the centre of the integrating sphere (sphere diameter of 500 mm) in such a way that its surface lies in the equatorial plane of the sphere. An internal lamp serves as a broadband light source; it does not, however, irradiate the sample directly. Due to the special construction, initially only the half-sphere of the sphere that lies behind the sample is irradiated. By a multitude of diffuse wall reflections on the internal coating, the radiation is transmitted into the half-space in front of the sample from which the sample is then irradiated from all directions with a constant radiance. Spectral selection is accomplished via a monochromator in the detection beam path.

A perfectly reflecting diffusor (PRD) at the sphere centre would have the same radiance as the wall of the half-space that irradiates it. Consequently, the measurement of the radiance of this hemisphere is equivalent to the measurement of the radiance of by the PRD. Since no reference standard is required, the Korte–Schmidt method provides an absolute measurement of the hemispherical reflectance.

3. BRDF measurements

3.1 Results overview

The data presented in this section is tabulated in Supplement 1. Figures 2 and 3 show the BRDF measurements made by the three laboratories as a function of the polar viewing angle, θ_d, for the white and grey samples, respectively. These values were calculated by averaging the measurements made at different values of the azimuthal viewing angle, ϕ_d in order to make the data easier to view. Because the samples are isotropic, there is only small variation over ϕ_d, which is considered later in this section.

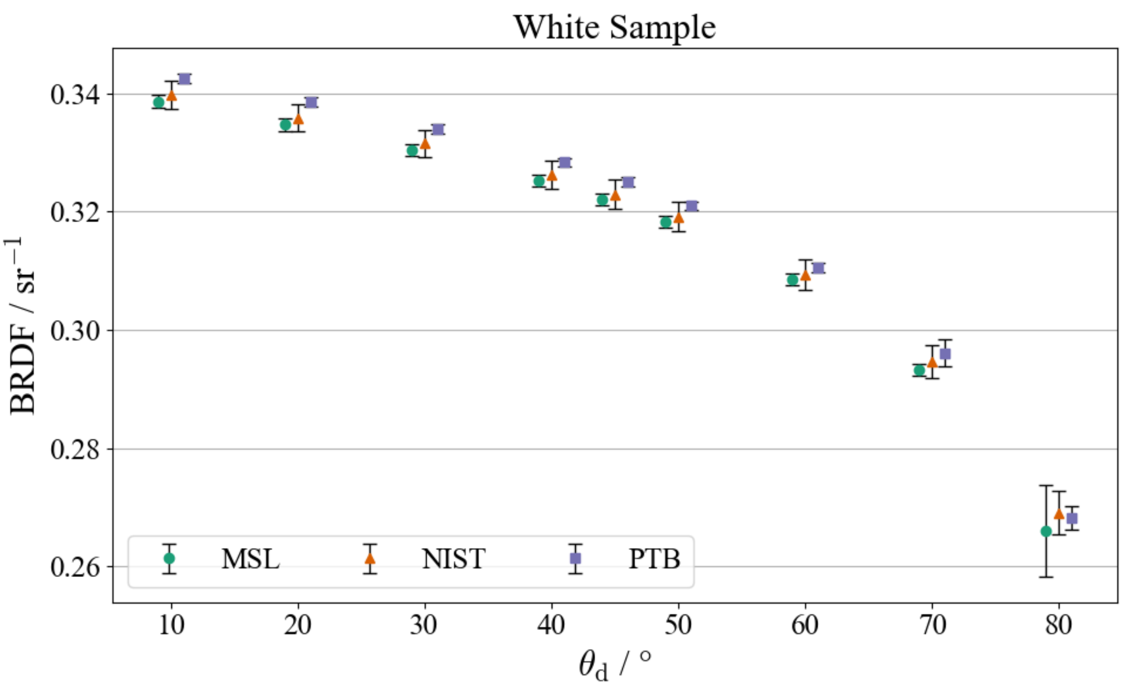

Figure 2. BRDF measurements of the white sample as a function of the polar viewing angle θ_d along with the corresponding expanded uncertainties. These values have been calculated after averaging the measurements made at different values of the azimuthal viewing angle, ϕ_d.

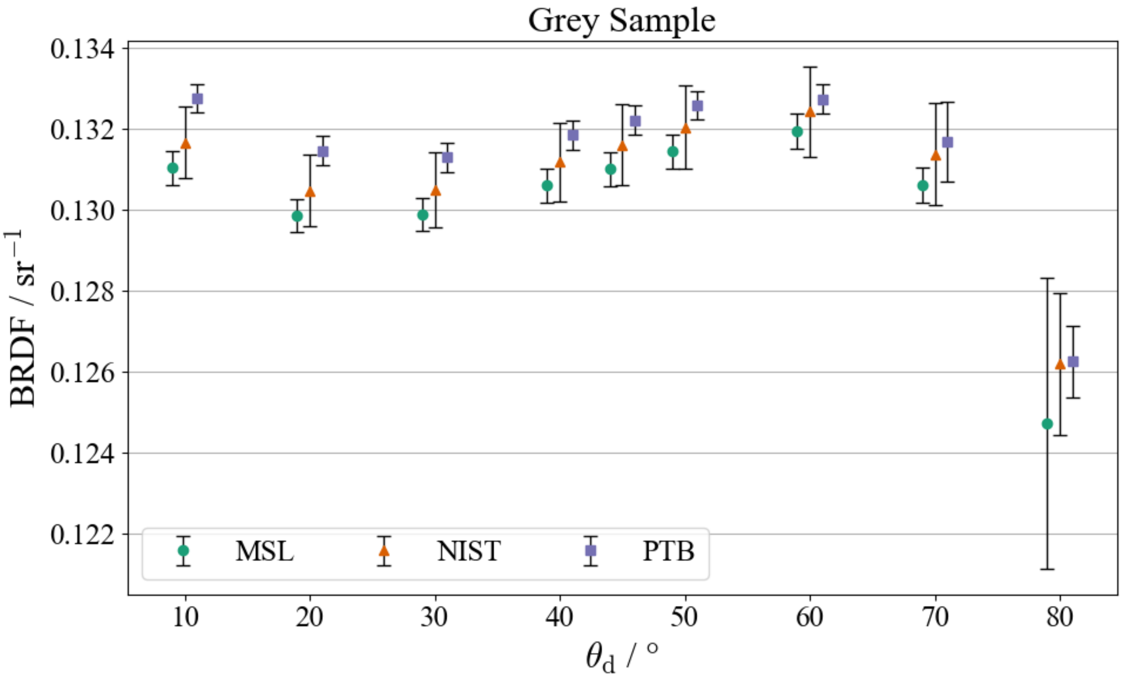

Figure 3. BRDF measurements of the grey sample as a function of the polar viewing angle θ_d along with the corresponding expanded uncertainties. These values have been calculated after averaging the measurements made at different values of the azimuthal viewing angle, ϕ_d.

Figures 4 and 5 show the degrees of equivalence with their corresponding expanded uncertainties as a function of the polar viewing angle θ_d for the white sample and the grey sample, respectively. These values have been calculated after averaging the measurements made at different values of the azimuthal viewing angle, ϕ_d. The reference value used in the calculations of the degrees of equivalence was the simple mean of the measurements from the three laboratories:

$$\zeta = \frac{\overline{f_\mathrm{r}^\mathrm{MSL}(\theta_\mathrm{d})}+\overline{f_\mathrm{r}^\mathrm{NIST}(\theta_\mathrm{d})}+\overline{f_\mathrm{r}^\mathrm{PTB}(\theta_\mathrm{d})}}{3}, \tag{4}$$

where $\overline{f_\mathrm{r}^l(\theta_\mathrm{d})}$ corresponds to the average BRDF value measured by a particular laboratory at a given θ_d (calculated by averaging the measurements made at the eight different azimuthal viewing angles). For laboratory l, the degrees of equivalence were then calculated as

$$\mathrm{DoE}_l = \overline{f_\mathrm{r}^l(\theta_\mathrm{d})} - \zeta. \tag{5}$$

The uncertainties in the reference value and the degrees of equivalence were calculated by propagating the measurement uncertainties through these equations with the assumption that the measurements made by the three laboratories were fully uncorrelated.

Across polar angles, a similar trend is observed for both samples, with MSL measuring values that are low, PTB measuring values that are high, and NIST generally in between. At smaller θ_d values, the NIST measurements are closer to the MSL measurements, with the PTB values higher. On the other hand, at larger θ_d values, the NIST values are closer to the PTB values. For all three laboratories, the uncertainties at $\theta_d = 70°$ and $\theta_d = 80°$ are considerably larger than those at lower angles.

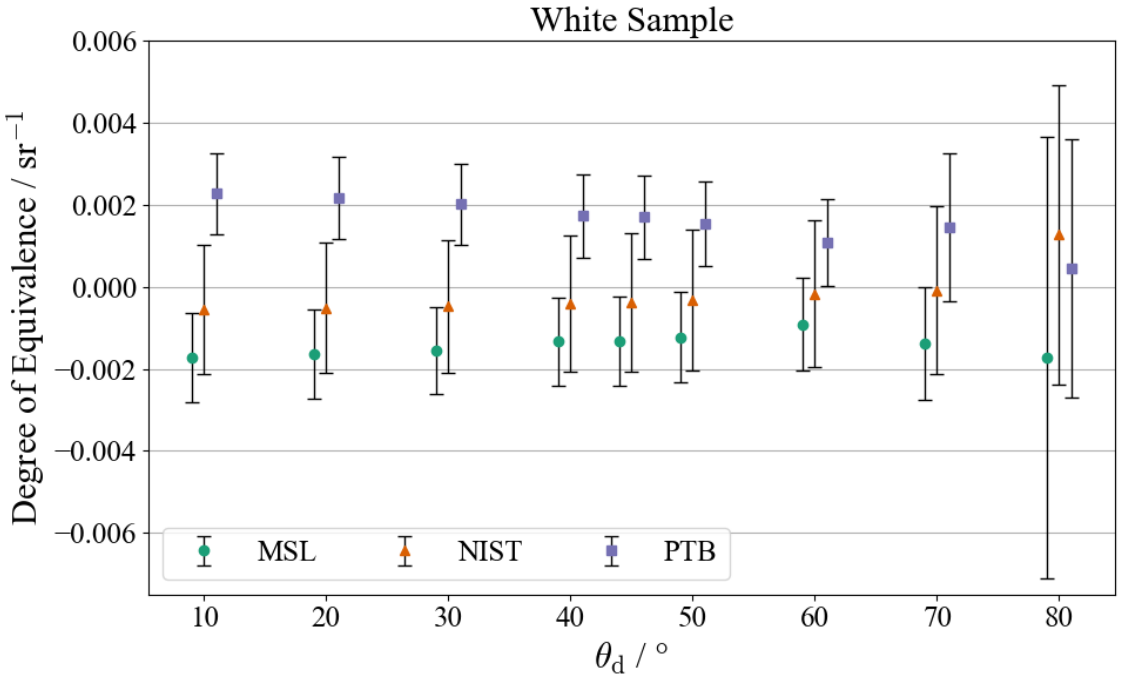

Figure 4. Degrees of equivalence for the white sample with the corresponding expanded uncertainties.

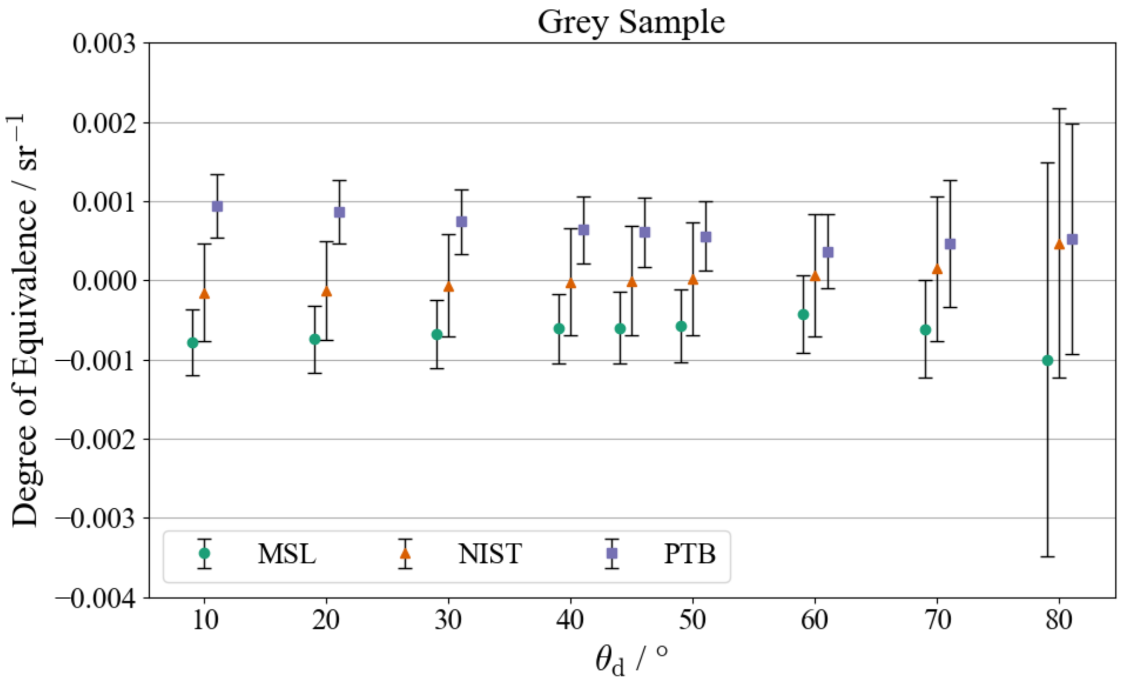

Figure 5. Degrees of equivalence for the grey sample with the corresponding expanded uncertainties.

Figures 6 and 7 show BRDF measurements of the white and grey samples, respectively, as a function of ϕ_d for $\theta_d = 20°$, $\theta_d = 45°$, and $\theta_d = 70°$ with the corresponding expanded uncertainties. Looking at the data for the white sample, we can see that when $\theta_d = 20°$, the MSL and NIST values agree well within the expanded uncertainties and follow a similar trend with respect to ϕ_d. On the other hand, the PTB measurements are higher with a different shape, just overlapping with the NIST values. A similar trend is observed at $\theta_d = 45°$ with the NIST measurements moving slightly towards the PTB values but still agreeing well with the MSL values. The relative uncertainties for all three participants increase significantly at $\theta_d = 70°$ compared to the other viewing angles, and it is difficult to identify a clear trend in BRDF with respect to ϕ_d.

For the grey sample, MSL and NIST generally show a similar shape with respect to ϕ_d at all three θ_d angles, with MSL again measuring values lower than NIST. PTB measures values that are higher and with a different shape with respect to ϕ_d at all three θ_d angles.

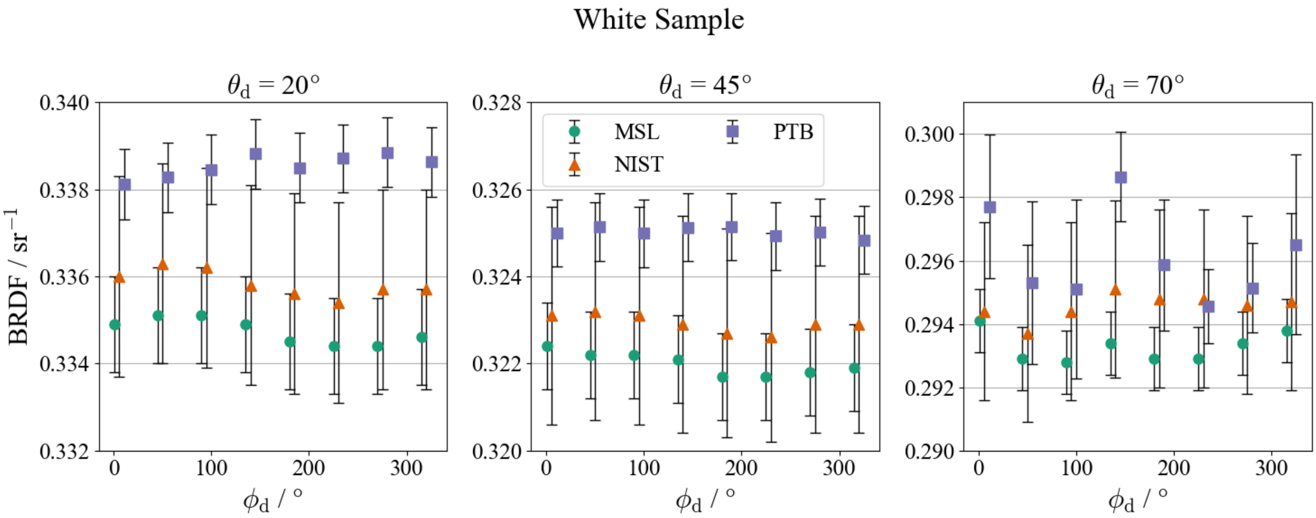

Figure 6. BRDF measurements and corresponding expanded uncertainties at $\theta_d = 20°$, $\theta_d = 45°$, and $\theta_d = 70°$ plotted against ϕ_d for the white sample.

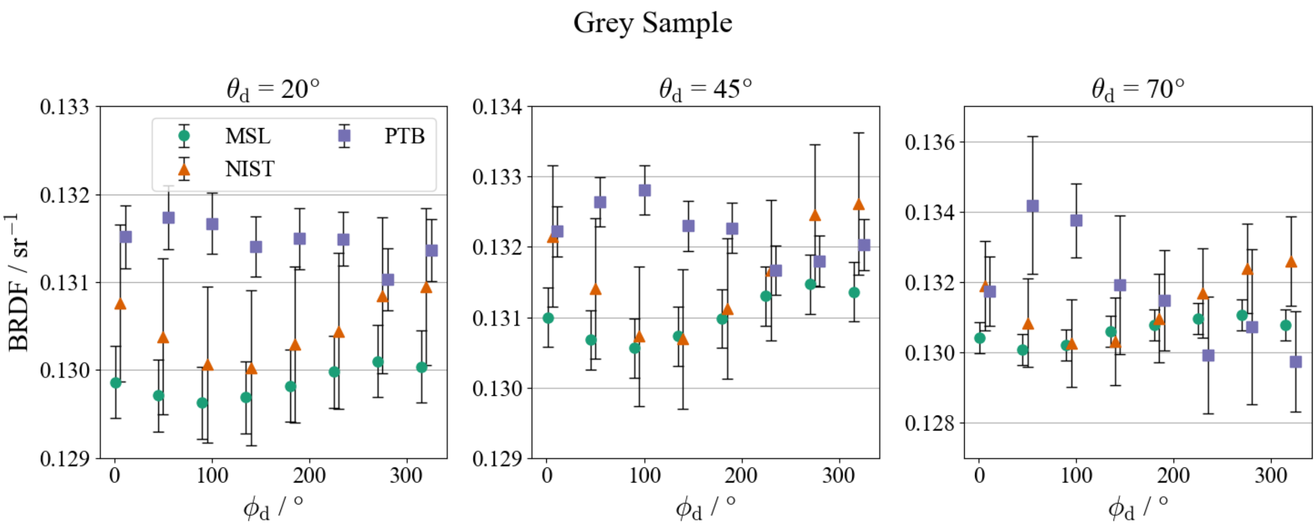

Figure 7. BRDF measurements and corresponding expanded uncertainties at $\theta_d = 20°$, $\theta_d = 45°$, and $\theta_d = 70°$ plotted against ϕ_d for the grey sample.

3.2 Uncertainties

Example uncertainty budgets for each of the three laboratories are presented in Tables 3, 4, and 5, which list the uncertainty contributions for the measurements of the white sample made at $\theta_d = 45°$, $\phi_d = 0°$. Some of the components, such as the alignment and angle setting, increase with θ_d. A full measurement model for the MSL goniospectrophotometer is available in [6], details on the NIST instrument is available in [7], and a detailed description of the PTB uncertainties is available in [11].

In this geometry, the dominant uncertainty contribution in the MSL measurements comes from the noise in the measurements, followed by the distance between the sample and the detector. For NIST, the largest uncertainty component is from the uniformity of the receiver. PTB's uncertainty budget is dominated by the nonlinearity of the detection system.

Table 3. MSL uncertainty budget for measurements made at $\theta_d = 45°$, $\phi_d = 0°$ for the samples. The uncertainty contributions are listed as absolute standard uncertainties.

Uncertainty Contribution	**White / sr^{-1}**	**Grey / sr^{-1}**
Noise	0.000 37	0.000 15
Length	0.000 26	0.000 11
Detector uniformity	0.000 19	0.000 079
Stray light	0.000 10	0.000 048
Aperture	0.000 046	0.000 019
Alignment	0.000 038	0.000 015
Angle setting	0.000 023	0.000 012
Gain ratio	0.000 005 5	0.000 002 2
Wavelength	0.000 004 4	0.000 002 3
View factor	0.000 000 064	0.000 000 002 6
Combined standard uncertainty	0.000 50	0.000 21
Expanded uncertainty ($k = 2$)	0.001 0	0.000 42

Table 4. NIST uncertainty budget for measurements made at $\theta_d = 45°$, $\phi_d = 0°$ for the samples. The uncertainty contributions are listed as absolute standard uncertainties.

Uncertainty Contribution	**White / sr^{-1}**	**Grey / sr^{-1}**
Receiver efficiency uniformity	0.001 0	0.000 42
Illumination centring	0.000 52	0.000 21
Viewing angle	0.000 32	0.000 13
Gain ratio	0.000 19	0.000 079
Finite solid angle calculation	0.000 16	0.000 066
Distance	0.000 097	0.000 040
Lock-in amplifier sensitivity ratio	0.000 065	0.000 026
Noise	0.000 032	0.000 013
Wavelength	<0.000 032	<0.000 013
Aperture area	0.000 002 2	0.000 000 9
Combined standard uncertainty	0.001 2	0.000 50
Expanded uncertainty ($k = 2$)	0.002 5	0.001 0

Table 5. PTB uncertainty budget for measurements made at $\theta_d = 45°$, $\phi_d = 0°$ for the samples. The uncertainty contributions are listed as absolute standard uncertainties.

Uncertainty Contribution	White / sr^{-1}	Grey / sr^{-1}
Nonlinearity of the detection system	0.000 35	0.000 14
Noise	0.000 15	0.000 12
Stability of radiance reflected by sample	0.000 13	0.000 19
Distance between light source and sample	0.000 12	0.000 049
Temperature difference between aperture and ambient	0.000 029	0.000 012
Irradiating area of the light source	0.000 019	0.000 0076
Stability of light source	<0.000 002 3	<0.000 0008
Combined standard uncertainty	0.000 39	0.000 18
Expanded uncertainty (k = 2)	0.000 78	0.000 36

3.3 Stability measurements

The comparison measurements were carried out by the three NMIs at various times between 2023 and 2025. To verify stability over that time, the samples were measured at MSL at the beginning of the comparison, in 2024, and again in 2025. Figure 8 shows the differences between the BRDF measurements made at $\theta_d = 45°$ as a function of ϕ_d for the two samples along with the expanded uncertainties in these differences (not including the shared effects between the three sets of measurements). Observed differences between the values measured in different years are consistent with insignificant drift in the samples, given the expanded uncertainty and noise component of the uncertainty in MSL's uncertainty budget. This indicates that there has been little drift in the samples over the period of the comparison measurements.

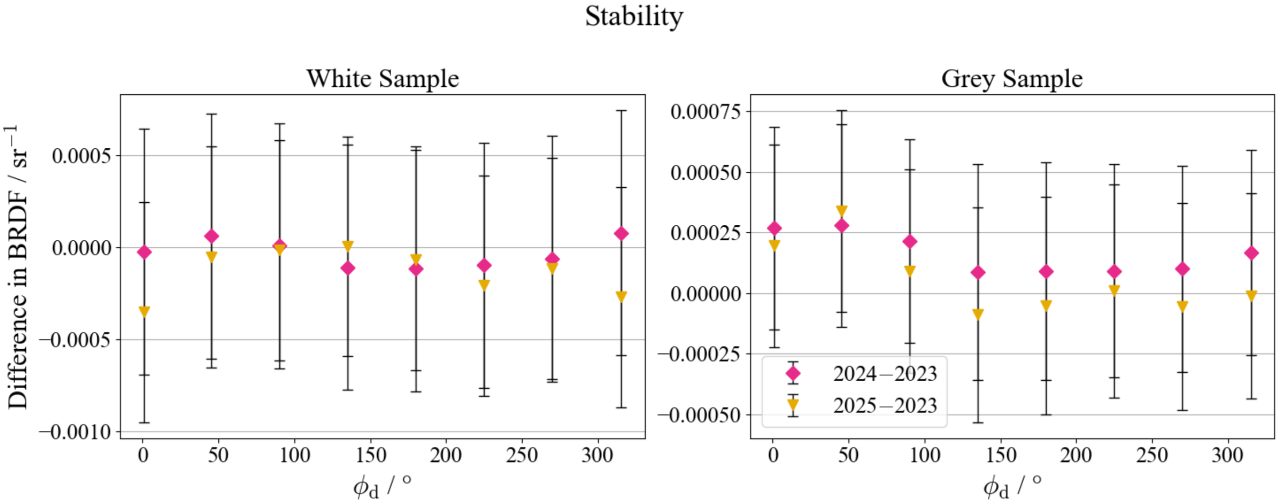

Figure 8. Differences between BRDF measurements made at MSL throughout the comparison at $\theta_d = 45°$ plotted against ϕ_d for the two samples, along with the corresponding expanded uncertainties.

4. Diffuse reflectance measurements

Measuring BRDF over the hemisphere allows the diffuse reflectance to be calculated through integration of the goniospectrophotometric measurements. The approach described in [6] was used for the integration.

Uncertainty due to the numerical method was negligible compared to uncertainty from other sources. Measurements of diffuse reflectance were also made using integrating spheres at NIST and PTB. MSL does not have a facility to measure absolute diffuse reflectance using an integrating sphere.

Table 6. Measurements of diffuse reflectance for the white and grey sample, made from integrating BRDF measurements and using an integrating sphere. The values in brackets indicate the expanded uncertainties in the last two digits.

Laboratory	White, integrated	White, sphere	Grey, integrated	Grey, sphere
MSL	0.9945 (37)		0.4095 (16)	
NIST	0.9984 (66)	0.9918 (40)	0.4113 (28)	0.4060 (16)
PTB	1.0041 (27)	0.9911 (20)	0.4135 (11)	0.4083 (20)

Table 6 shows the diffuse reflectance values for the two samples using both integrated BRDF measurements and direct integrating-sphere measurements. As expected from the BRDF measurements, MSL calculates the lowest diffuse reflectance value from the integrated BRDF measurements, with NIST calculating a slightly higher diffuse reflectance, and PTB higher again. For all three laboratories, the calculated diffuse reflectances are higher than the integrating-sphere measurements.

The ratio between the white sample's reflectance and the grey sample's reflectance is presented in Table 7 for each laboratory. The ratios for the integrated BRDF measurements agree well for all three laboratories, suggesting that the mechanism for differences in the integrated reflectance obtained by the three laboratories does not depend on the sample reflectance. Notably, the ratio for the PTB integrating sphere measurements is consistent with the ratio for integrated measurements found by all three laboratories, while the ratio for the NIST integrating sphere measurements is higher.

Table 7. Ratio between the white and grey sample diffuse reflectance measured by integrating BRDF measurements and using an integrating sphere for each laboratory. The values in brackets indicated the expanded uncertainties in the last two digits of the ratios.

Laboratory	White / grey, integrated	White / grey, sphere
MSL	2.429 (13)	
NIST	2.425 (23)	2.443 (14)
PTB	2.4283 (92)	2.427 (13)

5. Discussion and Conclusions

This paper has presented the results from a comparison of BRDF scales realised at three NMIs over the whole detection hemisphere for a white and a grey sintered PTFE sample. When averaged over ϕ_d, the trends in DoE of BRDF as a function of polar angle θ_d from the two samples were similar and reflect what has been observed in previous comparisons at a more limited set of geometries. The PTB BRDF scale is seen to be higher than the MSL BRDF scale, and the difference between the scales exceeds the $k = 2$ uncertainties for the smallest angles. The difference between the scales is within the $k = 2$ uncertainties for larger angles of detection, where measurement uncertainty is larger. The NIST BRDF scale lies between the MSL and PTB scales, trending closer to the MSL scale at lower polar angles, and to the PTB scale at higher angles, but in agreement with both. While the NIST result does not help resolve the scale differences between PTB and MSL, it is notable that the BRDF scale differences between PTB and MSL persisted over a broader range of geometries than previously explored [1, 2, 3]. Because NIST, unlike PTB and MSL, did not participate in the European Metrology Research Programme comparisons [2, 3], the results also serve to validate the consistency of NIST's BRDF scale with international consensus.

For the azimuthal dependence of the samples, the results are difficult to interpret. All three laboratories observed very little azimuthal dependence for the white sample, while for the grey sample, an azimuthal dependence can be observed in the data, but with PTB measuring a different shape compared to MSL and NIST. However, the azimuthal dependence in these samples was small relative to measurement uncertainties. Further study, possibly with samples that have a deliberate azimuthal dependence, is needed to understand the origins and significance of these differences.

The most striking difference between the instruments used at the three laboratories is the illumination method. Both MSL and NIST use the under-illumination scheme, while PTB uses the over-illumination scheme. This could be contributing towards the difference observed between the scales, with the MSL and NIST scales tending to agree, with PTB measuring higher BRDF values. The setups used for the two methods are quite different, so it is not practical for an instrument to change between the over- and under-illumination methods in order to test this theory.

Another difference between the instruments is the method for spectral determination. Both MSL and NIST use monochromatic illumination with broadband detection, while PTB uses broadband illumination and monochromatic detection. To test whether this is contributing to the differences observed, some tests were performed at MSL and PTB to measure with both monochromatic illumination and monochromatic detection by including cut-off filters in the beam path. However, no differences were observed between measurements made with both monochromatic illumination and detection compared with measurements made with only monochromatic selection on either the illumination or detection part. This indicates that the spectral determination is not contributing towards the observed differences.

By integrating the BRDF measurements to calculate the hemispherical diffuse reflectance of the samples and comparing them to measurements made using integrating spheres, this work also demonstrates the known discrepancy between integrating sphere and goniospectrophotometric realisations of hemispherical diffuse reflectance [5]. For the white sample, even the lowest diffuse reflectance value calculated by integrating the BRDF measurements is about 0.3% higher than the diffuse reflectance measured in the integrating spheres. Furthermore, the hemispherical diffuse reflectance is not expected to be larger than 1, but this value was obtained in one case. Even larger fractional differences between the sphere and goniospectrophotometric diffuse reflectance values is observed for the grey sample. While further study is needed, the difference in integrated values appears to arise from overall differences in the BRDF scales, rather than differences in a particular angular range, given that the three participants obtained roughly the same shape of BRDF with polar angle.

While the focus of this work was on comparison of the BRDF scales, the inclusion of integrating sphere measurements of diffuse reflectance revealed that the NIST and PTB integrating-sphere measurements agreed within $k = 2$ uncertainties for both samples. However, the ratio of the white sample reflectance to the grey sample reflectance was higher for the NIST integrating sphere than for PTB's sphere and the ratio obtained from integrating BRDF for all participants. Integrating spheres are known to be most accurate when the reflectance characteristics of the sample under test closely match that of the white sphere wall. Currently, a CCPR regional intercomparison of sphere-based directional hemispherical reflectance for greyscale samples is underway [12]. It is hoped that the results from this comparison will provide more insights into the sources of uncertainty in the measurements.

The results from this BRDF comparison demonstrate the current limits of agreement for BRDF measurements. Further work is needed to understand what is causing the differences between the scales. It would also be interesting to investigate differences between the BRDF scales for different types of material, for example, materials with a larger specular component.

Acknowledgements

The authors would like to thank Peter Saunders, Thomas Germer, Maritoni Litorja, and Catherine Cooksey for their careful review of the manuscript.

Disclosures Statement

The authors declare no conflicts of interest.

Data Availability

Data underlying the results presented in this paper are available in Supplement 1.

References

[1] C Cooksey, M Nadal, D Allen, *et al.* "Bidirectional reflectance scale comparison between NIST and PTB", *Applied Optics* **54** 4006–4015 (2015) https://doi.org/10.1364/AO.54.004006

[2] C Strothkamper, A Ferrero, A Koo, *et al.* "Multilateral spectral radiance factor scale comparison", *Applied Optics* **56** 1996–2006 (2017) https://doi.org/10.1364/AO.56.001996

[3] N Basic, E Molloy, A Koo, *et al.* "Intercomparison of bidirectional reflectance distribution function measurements at in- and out-of-plane geometries", *Applied Optics* **62** 13 (2023) https://doi.org/10.1364/AO.486156

[4] J C Zwinkels, T A Germer, B K Tsai, "Spectrophotometry: Accurate Measurement of Optical Properties of Materials", in *Experimental methods in the physical sciences*, Amsterdam, Elsevier (2014)

[5] M Nadal, K L Eckerle, E A Early, and Y Ohno, "Final report on the key comparison CCPR-K5: spectral diffuse reflectance", *Metrologia* **50**, 02003 (2013)

[6] E Molloy, A Koo, "MSL goniospectrophotometer measurement model", *Metrologia* **61** 025009 (2024) https://doi.org/10.1088/1681-7575/ad27de

[7] H J Patrick and C J Zarobila, "Ultraviolet to short-wave infrared spectral reflectance", NIST Special Publication 250–101 (NIST, 2024). https://doi.org/10.6028/NIST.SP.250-101

[8] D Hünerhoff, U Grusemann and A Höpe, "New robot-based gonioreflectometer for measuring spectral diffuse reflection", *Metrologia* **43** S11 (2006) https://doi.org/10.1088/0026-1394/43/2/S03

[9] KO Hauer and A Höpe, "High-grade uniform light source for radiometric and photometric applications", *MAPAN 24*, 175–182 (2009) https://doi.org/10.1007/s12647-009-0021-y

[10] H. Korte und M. Schmidt, "*Über Messungen des Leuchtdichtefaktors an beliebig reflektierenden Proben*", *Lichttechnik* **19**, 135A–137A (1967)

[11] I Santourian, T Quast, A Schirmacher, "Uncertainty budget for PTB's gonioreflectometers and ways to improve it in the short VIS spectral range", *Metrologia* **59** 025004 (2022) https://doi.org/ 10.1088/1681-7575/ac4e76

[12] *Bureau International des Poids et Mesures* (BIPM). APMP.PR-S7 "Spectral grey-scale diffuse reflectance", ongoing regional metrology organisation comparison. Entry in the Key Comparison Database. Available at: https://www.bipm.org/kcdb/comparison?id=1004